

# The tachocline and differential rotation in the Sun

Steven A. Balbus<sup>★†</sup> and Henrik N. Latter

*Laboratoire de Radioastronomie, École Normale Supérieure, 24 rue Lhomond, 75231 Paris Cedex 05, France*

Accepted 2010 May 25. Received 2010 May 19; in original form 2010 March 24

## ABSTRACT

In this paper, we present a model for the effects of the tachocline on the differential rotation in the solar convection zone. The mathematical technique relies on the assumption that entropy is nearly constant (‘well mixed’) in isorotation surfaces both outside and within the tachocline. The resulting solutions exhibit non-trivial features that strikingly resemble the true tachocline isorotation contours in unexpected detail. This strengthens the mathematical premises of the theory. The observed rotation pattern in the tachocline shows strong quadrupolar structure, an important feature that is explicitly used in constructing our solutions. The tachocline is treated locally as an interior boundary layer of small but finite thickness, and an explicit global solution is then constructed. A dynamical link can thus be established between the internal jump in the angular velocity at the tachocline and the spread of angular velocities observed near the solar surface. In general, our results suggest that the bulk of the solar convection zone is in thermal wind balance, and that simple quadrupolar stresses, local in radius, mediate the tachocline transition from differential rotation to uniform rotation in the radiative interior.

**Key words:** convection – hydrodynamics – Sun: helioseismology – Sun: rotation – stars: rotation.

## 1 INTRODUCTION

Recent work suggests that the isorotation contours in the bulk of the solar convection zone (SCZ) correspond to the characteristic curves of the vorticity equation in its ‘thermal wind’ form (Balbus 2009, hereafter B09; Balbus et al. 2009, hereafter BBLW; Balbus & Weiss 2010). In its undeveloped form, this equation relates entropy gradients to angular velocity gradients. The mathematical existence of the characteristics demands, therefore, some sort of functional relationship between the entropy  $S$  and angular velocity  $\Omega$ . The theory presented in the above papers is predicated upon the notion that within constant  $\Omega$  surfaces, the dominant, long-lived convective cells carry out their task of mixing entropy with great efficiency. This means that within a constant  $\Omega$  surface, the excess entropy gradient above and beyond the minimal radial gradient needed to maintain the convective state is, in essence, eliminated. The remaining ‘residual’ entropy is thus uniform in constant  $\Omega$  surfaces. More explicitly, the residual entropy  $S' \equiv S - S_r$  is formed by subtracting a function of spherical radius  $r$  (something close to the driving background entropy that has been averaged over angles), and  $S'$  is set equal to a function of  $\Omega$ . This is a powerful constraint, providing the necessary mathematical link for interpreting the solar isorotation contours as trajectory characteristics of a quasi-linear partial differential equation. BBLW advances several different lines of argument (heuristic, numeric and goodness of fit) supportive of this picture. Originally, a magnetohydrodynamics basis for the  $S - \Omega$  connection was put forth (B09), but the greater simplicity and generality, as well as the broad agreement with many different lines of argument, together suggest primacy for the BBLW mechanism.

An attractive feature of the theory presented in BBLW is that it provides simple and intuitive answers to not-so-trivial questions. For example, why can the SCZ not rotate on cylinders? Because if it did, then  $\Omega$  would necessarily depend upon the spherical colatitude angle  $\theta$ , therefore the entropy would also depend upon  $\theta$ , and this is inconsistent with a vanishing  $z$  gradient of  $\Omega$  in the thermal wind equation (TWE; cf. equation 2). Why then is  $\Omega$  dominated by its  $\theta$  gradient? Now we argue the other way: because the residual entropy has its dominant radial gradient removed (physically by mixing, mathematically by a simple subtraction), the relative importance of its  $\theta$  gradient has been enhanced. But residual entropy shares the same isosurfaces as  $\Omega$ . In numerical simulations, the fact that imposed latitudinal entropy gradients enforced at an interior boundary lead also to latitudinal gradients in  $\Omega$  (Miesch, Brun & Toomre 2006) becomes tautological: latitudinal  $S$  gradients lead inevitably to latitudinal  $\Omega$  gradients because these gradients are always counteraligned.

<sup>★</sup>E-mail: steven.balbus@lra.ens.fr

<sup>†</sup>Adjunct Professor, Department of Astronomy, University of Virginia, Charlottesville, VA 22903, USA.

In its current formulation, BBLW theory addresses the differential rotation in the Sun away from the tachocline. This is nothing if not prudent: the dynamics of the solar tachocline is a notoriously controversial and difficult topic (e.g. Hughes, Rosner & Weiss 2007). Yet, in studying the isorotation contours within the tachocline, one is struck both by the highly localized nature of the distortion and by the relative simplicity and uniformity of their appearance. In contrast to the bulk of the convection zone and the outer boundary layer, there is a sense of inevitability to these curves. Perhaps their gross form might not be sensitive to the complex details of the internal dynamical structure of the tachocline, any more than the gross adiabatic temperature profile of the SCZ depends upon the details of the convective heat flux. We might look instead to the exigencies of local forcing and to the strikingly quadrupolar structure of the region. The resulting mathematical demands of joining the isorotation contours in such a forced region to the overlying convective zone contours treated in BBLW may be sufficiently restrictive that the role of turbulence is tightly confined. In its current form, BBLW theory has too much ‘free play’: it needs to be restrained. In this paper, we will develop this point of view and pursue its consequences.

## 2 ANALYSIS

### 2.1 Trajectory and solution characteristics of the TWE

We follow the notation convention of BBLW. Cylindrical coordinates are denoted by radius  $R$ , azimuthal angle  $\phi$  and vertical coordinate  $z$ . The spherical coordinates are  $(r, \theta, \phi)$ , where  $r$  is the radius from the origin,  $\theta$  the colatitude angle and  $\phi$  the azimuthal angle. The angular velocity  $\Omega$ , pressure  $P$  and density  $\rho$  are understood to be azimuthal averages. The dimensionless entropy function  $\sigma$  is defined by

$$\sigma \equiv \ln P \rho^{-\gamma}, \quad (1)$$

where  $\gamma$  is the usual specific heat ratio or adiabatic index.

In SCZ applications, the TWE is the dominant balance of the vorticity equation, after azimuthal averaging, between the large-scale rotation and the baroclinic terms. The latter arises from a mismatch between equipotential (or isobaric) and isochoric surfaces. More specifically, contributions from convective turbulence are ignored (i.e. the convective Rossby number is small; Miesch & Toomre 2009), as are those from magnetic fields. The TWE for the convective zone is (e.g. Thompson et al. 2003; Miesch 2005; B09)

$$R \frac{\partial \Omega^2}{\partial z} = \frac{g}{\gamma r} \frac{\partial \sigma}{\partial \theta}, \quad (2)$$

where  $g = GM_{\odot}/r^2$ ; here  $G$  is the gravitational constant and  $M_{\odot}$  is a solar mass. In BBLW theory, there is a functional relationship of the form

$$\sigma' \equiv \sigma - \sigma_r = f(\Omega^2), \quad (3)$$

where  $\sigma_r$  is any function of  $r$  (in practice something very close to an angle-averaged  $\sigma$ ) and  $f$  is an unspecified function. Replacing  $\sigma'$  by  $\sigma$  does not alter the TWE, and with the aid of equation (3), the TWE (equation 2) becomes

$$\frac{\partial \Omega^2}{\partial r} - \left( \frac{gf'}{\gamma r^2 \sin \theta \cos \theta} + \frac{\tan \theta}{r} \right) \frac{\partial \Omega^2}{\partial \theta} = 0, \quad (4)$$

where  $f' = df/d\Omega^2$ . In this paper, we wish to retain, at least in a formal sense, the tachocline meridional stress  $T(r, \theta)$  on the right-hand side of the equation<sup>1</sup>:

$$\frac{\partial \Omega^2}{\partial r} - \left( \frac{gf'}{\gamma r^2 \sin \theta \cos \theta} + \frac{\tan \theta}{r} \right) \frac{\partial \Omega^2}{\partial \theta} = T(r, \theta). \quad (5)$$

Although  $T$  is certainly poorly understood in detail, there is presumably *some* function of position that makes equation (5) correct. The point is that the ensuing formal solution is not without content. The angular velocity  $\Omega^2$  satisfies

$$\frac{d\Omega^2}{dr} = T(r, \theta) \quad (6)$$

$$\frac{d\theta}{dr} = -\frac{gf'(\Omega^2)}{\gamma r^2 \sin \theta \cos \theta} - \frac{\tan \theta}{r}. \quad (7)$$

In other words, to solve for  $\Omega(r, \theta)$ , we use the contours as defined by the characteristic differential equation of BBLW theory; along these contours  $\Omega$  changes according to equation (6).

We shall assume that equation (3) is valid both in the bulk of the convective zone and in the tachocline. This is by no means obvious. The low Rossby number approximation is likely to hold well in the tachocline, and convective rolls should be strongly affected by shear. But since the turbulent stresses in the tachocline are very different from those in the convective zone, even if such a functional relationship holds, the function  $f$  may in principle be quite different in the two regions.

<sup>1</sup> In passing from the lower convective zone into the radiative layers, the baroclinic term proportional to  $(\partial P/\partial \theta)(\partial \sigma/\partial r)$  should be formally be retained in our equation. As a practical matter, the rotational pattern is essentially spherical in this region, and the dominant balance is between the inertial terms and the external stress. (We thank the referee M. Miesch for drawing our attention to this point.)

On the other hand *everything* changes in the two regions, not the least of which is the sudden appearance of the stresses themselves. For the class of solutions we consider here (which reproduce the data strikingly well), a change in  $f'$  cannot be disentangled from a change in  $T$ , a point we will explicitly discuss (Section 2.6). Hence, we retain the functional equation (3) throughout the convective zone and the tachocline.

Note that, in contrast to the vanishing  $T$  limit, when  $T$  is finite  $f'(\Omega^2)$  is generally *not* constant along the characteristic. But this does not mean that there is nothing to be learned from considering the limit of constant  $f'$  as a special case for the current, more general, problem. Indeed, in our first approach we should keep formalism to a minimum. It has been earlier noted (B09) that choosing  $f'(\Omega^2)$  to be a global constant captures important semiquantitative features of the true SCZ isorotation contours, so let us begin first with this mathematically simple case. We will then be poised to look at a more complex problem.

## 2.2 $f'(\Omega^2) = \text{constant}$

In the limit of constant  $f'$ , the formal trajectory characteristics are identical to those in BBLW theory, both outside and within the tachocline:

$$\sin^2 \theta = \frac{r_0^2}{r^2} \sin^2 \theta_0 + \frac{2f'GM_\odot}{r^2\gamma} \left( \frac{1}{r} - \frac{1}{r_0} \right), \quad (8)$$

where  $r_0$  is the radius at which  $\Omega$  is initially specified (generally near or at the surface) and  $\theta_0$  marks the beginning value of  $\theta$  for a particular characteristic path. The sign of  $T$  is clear: following a BBLW characteristic,  $T$  must be negative at high latitudes and positive at equatorial latitudes. Along such a characteristic, denoted  $\theta(r)$ ,  $\Omega^2$  is given by

$$\Omega^2 = \Omega_0^2 + \int_{r_0}^r T[r, \theta(r)] dr, \quad (9)$$

where  $\Omega_0$  is the value of  $\Omega$  at the defining surface. (Note that  $r_0$ , which is generally taken at or near the surface, may be larger than  $r$ .) The formal solution (9) is in fact general for any  $f'$ , provided that  $\theta(r)$  is taken to be the proper trajectory characteristic.

It is not difficult to extract the qualitative behavior of  $\Omega$  from equations (8) and (9). The stress  $T$  is very small except in a very narrow region near the transition radius  $r_T$ . Thus  $\Omega^2$  remains essentially fixed at its initial value  $\Omega_0^2$  along most of the extent of the characteristic. This, of course, is BBLW theory. Then, there is a sudden increase in  $T$  very near  $r_T$ , and along the BBLW characteristic  $\theta(r)$ ,  $\Omega$  now makes a very sharp rise (or a sharp drop near the equator) as it settles to the uniform rotation rate in the radiative interior.

The resulting isorotational curves can be understood with the aid of Fig. 1. This diagram is a local representation of the SCZ–tachocline boundary in a region where the angular velocity begins to increase sharply moving inward. The radius  $r$  increases upward to the right-hand side;  $\theta$  increases downward to the right-hand side. The numbers 1' through 4' label BBLW characteristics, which, in the convection zone, are precisely the isorotation contours. Hence these numbers may also be thought of as angular velocities, increasing with the magnitude of the number.

Consider the rightmost contour labelled 4'. Between 4' and the dot labelled 4 on the same curve, the contour passes through the convective zone, and the angular velocity remains constant. Dot 4 marks the beginning of the tachocline and a steep rise in the angular velocity. To continue the trace of the isorotation contour, a sharp turn to the (reader's) left-hand side is required, and the curve continues by passing through dot 4 on the curves labelled 3', 2' and 1', etc. Thus, within the narrow radial band of changing  $\Omega$ , if one were to follow curves of constant  $\Omega$ , from one BBLW trajectory characteristic to those immediately adjacent, a quasi-spherical ( $r$  increases somewhat with  $\theta$ ) path would emerge. This abrupt change in the isorotation contours is clearly seen in the helioseismology data. A more delicate  $\theta$  dependence of  $r$  is also present in the data, though this may be an artefact of the inversion technique.

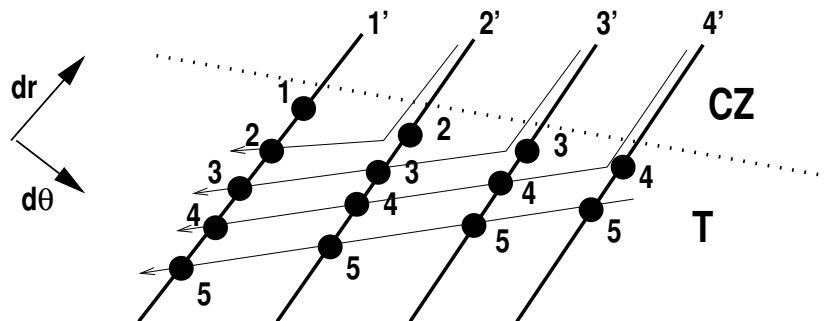


**Figure 1.** Schematic local rendering of the isorotation contours in the presence of tachocline meridional stress. CZ denotes the convective zone and T denotes the tachocline. The thick curves labelled 1', 2', etc. are the CZ isorotation contours in BBLW theory. Numbers may be thought of as representing the relative ordering of fiducial  $\Omega$  values. The presence of the tachocline, indicated by black dots, is to increase  $\Omega$  along what was an isorotation contour. The new, proper isorotation contours (thin lines) resemble those seen in the helioseismology data: quasi-spherical, with an increase in  $r$  as  $\theta$  increases, and with a sharply angled upward turn towards the surface.

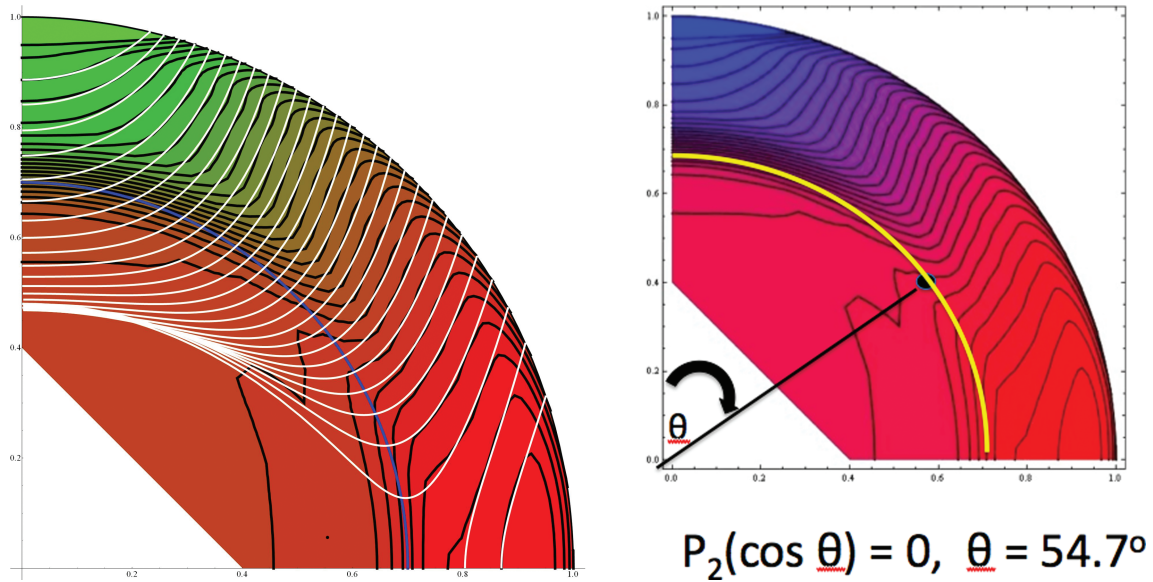


**Figure 2.** Left-hand panel: constant  $\Omega$  contours (light) of the TWE from BBLW theory overlaid on top of (dark) isorotation contours (GONG data, courtesy of R. Howe). Inner dark quarter circle is the bottom edge of the convective zone. Right-hand panel: tachocline is absent when  $P_2(\cos \theta) = 0$ , consistent with quadrupole structure.

### 2.3 Green's function solution

The above description motivates a Green's function approach. Consider a tachocline stress of the form

$$T(r, \theta) = -(\Delta\Omega^2)F(\theta)\delta(r - r_T), \quad (10)$$

where  $\Delta\Omega^2$  is the 'jump amplitude',  $F(\theta)$  is a function of  $\theta$  that modulates the magnitude of the radial inward jump ( $F$  is positive at high latitudes, negative at small latitudes) and  $\delta(r - r_T)$  is the Dirac delta function. Then along a BBLW characteristic,

$$\Omega^2 = \Omega_0^2 + \Theta(r_T - r)(\Delta\Omega^2)F[\theta(r_T)], \quad (11)$$

where  $\theta(r)$  may be determined explicitly from equation (8) and  $\Theta(x)$  is the Heaviside function. (Recall that  $\Theta$  is unity when its argument is positive and zero when its argument is negative.) In this rather drastic idealization, BBLW theory breaks down at a single radius  $r_T$ , which we identify with the tachocline. The BBLW isorotation contours change abruptly to a single spherical shell in this model, compressing the entire tachocline down to a range of vanishing thickness.

### 2.4 Quadrupole structure

It is possible, of course, to continue along the lines of the previous section by introducing progressively more sophisticated models for  $T(r, \theta)$  and  $f'(\Omega^2)$ , and in fact we shall shortly consider the case in which  $f'$  is a linear function of  $\Omega^2$ . It is already clear, however, that within this scheme, the helioseismology data can be reproduced – at least qualitatively. If our approach is not quite tight enough to be broadly predictive, it might be more profitably applied in the reverse sense: use the solar rotation data directly to infer the form of  $T(r, \theta)$ .

A very important result emerges immediately. In Fig. 2, on the left-hand panel we see the isorotation contours taken from GONG data,<sup>2</sup> together with the BBLW characteristics overlaid for reference. As one passes through the tachocline from larger to smaller radii, the inward jump in  $\Omega^2$  changes from positive to negative for  $\theta$  larger than  $54.7^\circ$ , the value of  $\theta$  for which  $\cos^2 \theta = 1/3$ . The inset to the right-hand side in Fig. 2, displaying GONG data together with the location of the critical angle, shows this very clearly. The magnitude of the jump then grows (in the negative sense) as  $\theta$  increases, as we move towards the equator. The spacing of the isorotational contours is, at least crudely, about half the interval at the poles as compared with the equator. Even granting the inevitable uncertainties associated with the polar data (which are not reliable poleward of  $70^\circ$ ), these results are much what one would expect if  $F(\theta)$ , the angular component in our radially local model, were proportional to

$$P_2(\cos \theta) = \frac{1}{2}(3 \cos^2 \theta - 1),$$

the Legendre polynomial of order 2. To leading order, the tachocline stresses are revealing a *dominant quadrupolar* structure.

This is such a fundamental property of tachocline structure, it is curious that the near coincidence of the zero of  $P_2(\cos \theta)$  and the 'zero' of the tachocline has not been emphasized in the earlier literature. While meridional flows and their associated stresses have been an important feature of dynamical models of the tachocline (e.g. Spiegel & Zahn 1992; Gough & McIntyre 1998), and such flows are generally associated

<sup>2</sup> We thank R. Howe for providing us with these results.

with  $P_2(\cos \theta)$  stresses (Schwarzschild 1958), what is striking here is the manifest quadrupolar morphology. In Section 2.6 we use explicit quadrupolar forcing to leverage a mathematically precise isorotational contour solution from our fundamental equation, with essentially no other input. So it is of some interest to try to understand its origin.

The most important omission from the TWE, the basis of our analysis, is the contribution from turbulent stresses and meridional flow. These may be kinetic or magnetic, but they will generally take the form of a sum of terms proportional to

$$\partial_i(V_i W_\phi / R),$$

where the index  $i$  is itself summed over and  $V$  and  $W$  represent symbolic vector quantities (velocity fluctuations, vorticity, current density, etc.). It is the  $r$  and  $\theta$  components of  $i$  that are important (the  $\phi$  components vanish either explicitly or upon azimuthal averaging); hence the earlier designation of the resulting stress as ‘meridional’. The net contribution of these correlated products evidently behaves as a large-scale quadrupolar forcing. Given the symmetry of our flow, it is not surprising that the leading-order departure from spherical structure is quadrupolar, but it is rather surprising how well this approximation works.

## 2.5 $F(\theta) = P_2(\cos \theta)$ : an explicit solution

We now combine the results of the previous section to obtain an explicit mathematical solution for  $\Omega$ . Equation (8) implies quite generally that

$$\sin^2 \theta_0 = \frac{r^2}{r_0^2} \sin^2 \theta - \frac{2f'GM_\odot}{r_0^2\gamma} \left( \frac{1}{r} - \frac{1}{r_0} \right). \quad (12)$$

Now at  $r = r_T$  equation (8) gives

$$\sin^2 \theta(r_T) = \frac{r_0^2}{r_T^2} \sin^2 \theta_0 + \frac{2f'GM_\odot}{r_T^2\gamma} \left( \frac{1}{r_T} - \frac{1}{r_0} \right). \quad (13)$$

Then, substituting equation (12) in (13) leads to

$$\sin^2 \theta(r_T) = \frac{r^2}{r_T^2} \sin^2 \theta + \frac{2f'GM_\odot}{r_T^2\gamma} \left( \frac{1}{r_T} - \frac{1}{r} \right) \quad (14)$$

or

$$\cos^2 \theta(r_T) = \left( 1 - \frac{r^2}{r_T^2} \right) \sin^2 \theta + \frac{2f'GM_\odot}{r_T^2\gamma} \left( \frac{1}{r} - \frac{1}{r_T} \right). \quad (15)$$

Then, equation (11) becomes

$$\Omega^2(r, \theta) = \Omega_0^2 \left( \sin^2 \theta_0 \right) + \Theta(r_T - r)(\Delta\Omega^2)P_2[\cos \theta(r_T)], \quad (16)$$

where  $\sin^2 \theta_0$  is given by equation (12),  $\cos \theta(r_T)$  by equation (15), and we have assumed that  $F$  is the Legendre polynomial of order 2.

Equation (16) is the desired explicit solution for  $\Omega^2$ , but there is another way to formulate the content of our simple problem: given  $\Delta\Omega^2$ , what kind of a spread of surface velocities is associated with this jump? The answer is

$$\Omega_0^2 \left( \sin^2 \theta_0 \right) = \Omega_{\text{rad}}^2 - (\Delta\Omega^2)P_2[\cos \theta(r_T)] = \Omega^2 - (\Delta\Omega^2) + \frac{3}{2}(\Delta\Omega^2) \sin^2[\theta(r_T)], \quad (17)$$

where  $\Omega_{\text{rad}}$  is the angular velocity of the uniformly rotating radiative interior. With the aid of equation (13), we may rewrite this in terms of  $\sin^2 \theta_0$ . Choosing  $r_0^2/r_T^2 = 2$ , and denoting the final term of equation (13) as  $\xi$  (a number of the order of, but typically less than, unity), we find

$$\Omega_0^2 \left( \sin^2 \theta_0 \right) = \Omega_{\text{rad}}^2 - (1 + \xi)(\Delta\Omega^2) + 3(\Delta\Omega^2) \sin^2(\theta_0). \quad (18)$$

This calculation is a bit too simple to generate more complexity than a  $\sin^2 \theta_0$  departure from uniform surface rotation. Nevertheless, for reasonable values of  $\Delta\Omega^2$ , equation (18) gives a very respectable rendering of a solar-like surface rotation profile. More importantly, it establishes a dynamical coupling between the spread in  $\Omega^2$  present near the surface and the jump in  $\Omega^2$  at the location of tachocline. The connection between these two regions is possible because of the existence of linking trajectory characteristics.

Equation (18) should not be construed as a statement that the spread in surface angular velocities is actually *caused* by forcing from the tachocline; indeed, the sense of causality is generally thought to run in the opposite sense: from the SCZ to the tachocline (e.g. Gough 2010). Instead, equation (18) shows explicitly how the dynamics of thermal wind balance plus external driving leads to a relatively simple coupling between the radial jump in  $\Omega^2$  at the tachocline and the angular spread in  $\Omega^2$  at the surface.

## 2.6 $f'(\Omega^2)$ linear in $\Omega^2$

### 2.6.1 Governing equation

We next consider the case in which  $f'$  varies linearly with  $\Omega^2$ . This is useful both in establishing that there is no particular sensitivity to the assumption of a constant  $f'$  and in allowing more detailed structure to be revealed. In fact, the essential qualitative effects of a non-constant  $f'$  will be evident once the governing equation is at hand.

We begin by rewriting the trajectory characteristic equation (7) in the compact form

$$\frac{dR^2}{dr} = -\frac{2g}{\gamma} f'(\Omega^2), \quad (19)$$

where, as before,  $R = r \sin \theta$ , the axial radius. Let

$$f'(\Omega^2) = -\alpha - \beta \Omega^2, \quad (20)$$

where  $\alpha$  and  $\beta$  are constants. Dividing by  $g$ , differentiating with respect to  $r$  and using equations (20) and (6) leads to

$$\frac{d}{dr} \frac{1}{g} \frac{dR^2}{dr} = \frac{2\beta}{\gamma} T(r, \theta). \quad (21)$$

Recalling that  $g = GM_{\odot}/r^2$ , this leads to the final form of our equation for the trajectory characteristics, now free of all explicit  $\Omega$  dependence:

$$\frac{d^2}{dr^2} (rR^2) = \frac{2\beta GM_{\odot}}{\gamma r} T(r, \theta). \quad (22)$$

We now make the very reasonable and important assumption that  $T(r, \theta)$  is local in  $r$ , so that this variable is always near the shell  $r = r_T$  whenever  $T$  is finite. In essence, we ignore curvature terms, something we must do self-consistently since these global terms are not known for general  $T(r, \theta)$ . The local model avoids this difficulty while retaining the essential physics because the tachocline transition is not, in reality, very broad.

Consider equation (22) when the driving term  $T(r, \theta)$  takes the (radially local) form

$$T(r, \theta) = -T_0 P_2(\cos \theta), \quad (23)$$

where  $T_0$  is a constant term. We assume that  $T$  is present only for  $r < r_T$ . In this region, the differential equation (22) becomes

$$\frac{d^2(r^3 \sin^2 \theta)}{dr^2} = \frac{2\beta GM_{\odot} T_0}{\gamma r} \left( \frac{3}{2} \sin^2 \theta - 1 \right). \quad (24)$$

It should be noted that the function  $f'$  makes its appearance here only through the  $\beta$  parameter, and then only via the combination  $\beta T_0$ . This illustrates the point first made in Section 1: a different value of  $\beta$  can equivalently be regarded as keeping  $\beta$  the same and changing  $T_0$ . There is nothing to be gained by allowing a change in  $f'$  in the tachocline, at least not for the class of model of interest here.

Replacing  $r$  by  $r_T$  everywhere leads to the differential equation

$$\frac{d^2(\sin^2 \theta)}{dr^2} = \frac{3\beta GM_{\odot} T_0}{\gamma r_T^4} \left( \sin^2 \theta - \frac{2}{3} \right) \equiv k^2 \left( \sin^2 \theta - \frac{2}{3} \right). \quad (25)$$

This is a *linear* second-order equation for  $\sin^2 \theta$ , and the solution is

$$\sin^2 \theta = A_1 \cosh(kr) + A_2 \sinh(kr) + \frac{2}{3}, \quad (26)$$

where  $A_1$  and  $A_2$  are integration constants to be determined.<sup>3</sup>

### 2.6.2 Global solution

The characteristic solution for  $r > r_T$  is already known (BBLW):

$$\sin^2 \theta = \frac{r_0^2}{r^2} \sin^2 \theta_0 + \frac{2GM_{\odot} f'(\Omega_0^2)}{\gamma r^2} \left( \frac{1}{r} - \frac{1}{r_0} \right), \quad (27)$$

where

$$\Omega_0^2 (\sin^2 \theta_0) = \Omega_1^2 + \Omega_2^2 \sin^2 \theta_0 \quad (28)$$

and  $\Omega_1^2$  and  $\Omega_2^2$  are fixed constants.

We seek global solutions in which the exterior solution (27) for  $r > r_T$  joins smoothly to the interior solution (26) for  $r < r_T$  at  $r = r_T$ . The solution for  $\sin^2 \theta$  and its first derivative with respect to  $r$  should be continuous. Two dimensionless parameters are needed, defined by

$$\xi_1 = \frac{2GM_{\odot} \beta \Omega_2^2}{\gamma r_T^3}, \quad (29)$$

$$\xi_2 = \frac{2GM_{\odot} (\alpha + \beta \Omega_1^2)}{\gamma r_T^3}. \quad (30)$$

<sup>3</sup> Equation (24) may in fact be solved analytically without making the local approximation. But since locality has been used implicitly in ignoring the radial structure in  $T$ , it is best to be self-consistent.

An easy way to determine representative values of  $\xi_1$  and  $\xi_2$  is to use the  $B$  parameter introduced in B09 for solving for the form of the SCZ isorotation curves:

$$-\frac{B}{r_0^3} \equiv -\frac{2GM_\odot f'(\Omega_0^2)\Omega_0^2}{\gamma r_0^3}. \quad (31)$$

(Note that the solar radius notation  $r_\odot$  was used in B09 instead of our  $r_0$ .) A very simple and reasonable SCZ model is discussed in B09 using

$$-\frac{B}{r_0^3} = 0.12 + 0.8 \sin^2 \theta_0, \quad (32)$$

which would imply

$$\xi_1 = \left(\frac{r_0}{r_T}\right)^3 0.8, \quad \xi_2 = \left(\frac{r_0}{r_T}\right)^3 0.12. \quad (33)$$

Two other parameter combinations may be defined that will be useful later:

$$\xi_3 = \left(\frac{r_0}{r_T}\right)^2 - \left[1 - \left(\frac{r_T}{r_0}\right)\right] \xi_1, \quad (34)$$

$$\xi_4 = \xi_2 \left[1 - \left(\frac{r_T}{r_0}\right)\right]. \quad (35)$$

At  $r = r_T$ , the second derivative of  $\sin^2 \theta$  along a characteristic is discontinuous, but its value and first derivative are continuous. With equations (26) and (27), together with the  $\xi$  parameters, these two continuity conditions may be written as

$$\xi_3 \sin^2 \theta_0 - \xi_4 = A_1 \cosh kr_T + A_2 \sinh kr_T + \frac{2}{3}, \quad (36)$$

$$(\xi_1 - 2\xi_3) \sin^2 \theta_0 + \xi_2 + 2\xi_4 = kr_T(A_1 \sinh kr_T + A_2 \cosh kr_T). \quad (37)$$

Solving for  $A_1$  and  $A_2$ , we find the following interior solution for the characteristics:

$$\sin^2 \theta - \frac{2}{3} = \left(\xi_3 \sin^2 \theta_0 - \xi_4 - 2/3\right) \cosh k(r_T - r) - \frac{\sinh k(r_T - r)}{kr_T} [(\xi_1 - 2\xi_3) \sin^2 \theta_0 + \xi_2 + 2\xi_4]. \quad (38)$$

For future reference, we list here the form of this characteristic, isolating  $\sin^2 \theta_0$ :

$$\sin^2 \theta_0 = \frac{\sin^2 \theta - 2/3 + (\xi_4 + 2/3) \cosh k(r_T - r) + \sinh k(r_T - r)(\xi_2 + 2\xi_4)/kr_T}{\xi_3 \cosh k(r_T - r) + \sinh k(r_T - r)(2\xi_3 - \xi_1)/kr_T}. \quad (39)$$

To solve for  $\Omega^2$  along the characteristic (38), use equation (9), noting that  $T(r, \theta)$  vanishes for  $r_0 > r > r_T$ :

$$\Omega^2 = \Omega_0^2 - \int_r^{r_T} T(r, \theta) dr = \Omega_0^2 + \frac{3T_0}{2} \int_r^{r_T} [\sin^2 \theta(r) - 2/3] dr. \quad (40)$$

Integrating with the help of equation (38), we obtain

$$\Omega^2 = \Omega_0^2 + \frac{3T_0}{2} \left\{ [(\xi_1 - 2\xi_3) \sin^2 \theta_0 + \xi_2 + 2\xi_4] \left(1/k^2 r_T\right) [\cosh k(r_T - r) - 1] - (\xi_3 \sin^2 \theta_0 - \xi_4 - 2/3) (1/k) \sinh k(r_T - r) \right\}. \quad (41)$$

This gives us the solution along the characteristic beginning at the surface value  $\Omega_0^2$ , which is itself a function of  $\sin^2 \theta_0$ . We would like to have an expression for  $\Omega^2(r, \theta)$ , without reference to the characteristics, so that we may obtain the isorotation contours. To this end, we first use equation (28) to expand  $\Omega_0^2$ , followed by equation (39) to eliminate  $\sin^2 \theta_0$  from the above expression. In this way, we may obtain the desired isorotation contours in the form of  $\sin^2 \theta$  as a function of  $\Omega^2$  and  $r$  (as well as the various parameters of course). The result of this rather lengthy algebraic excursion is that the isorotation contours in the tachocline are given by

$$\sin^2 \theta - \frac{2}{3} = \frac{H_1 - H_2 + H_3}{1 - H_4}, \quad (42)$$

where

$$H_1 = \frac{\Omega^2 - \Omega_1^2}{\Omega_2^2} \left[ \xi_3 \cosh k(r_T - r) + (2\xi_3 - \xi_1) \frac{\sinh k(r_T - r)}{kr_T} \right], \quad (43)$$

$$H_2 = [(\xi_4 + 2/3) \cosh k(r_T - r) + (\xi_2 + 2\xi_4)(1/kr_T) \sinh k(r_T - r)], \quad (44)$$

$$H_3 = [\xi_3(\xi_2 + 2\xi_4) - (\xi_2 + 2/3)(2\xi_3 - \xi_1)] \frac{\cosh k(r_T - r) - 1}{\xi_1} \quad (45)$$

and

$$H_4 = \frac{kr_T}{\xi_1} \left[ \xi_3 \sinh k(r_T - r) + \frac{(2\xi_3 - \xi_1)(\cosh k(r_T - r) - 1)}{kr_T} \right]. \quad (46)$$

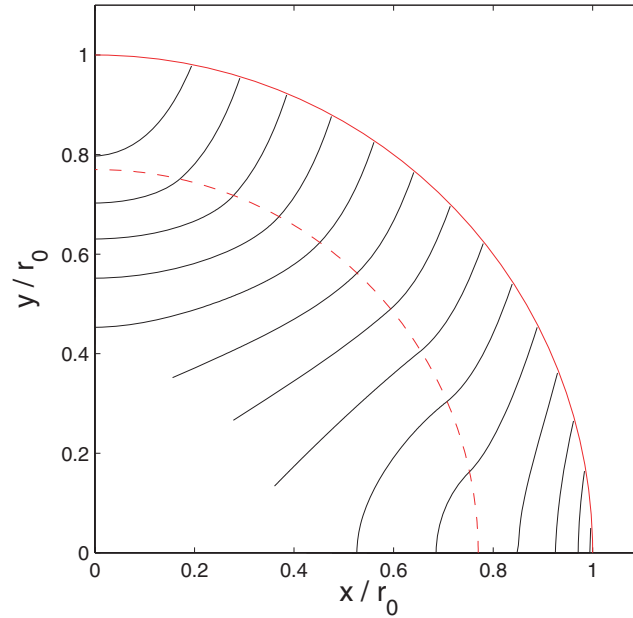


**Figure 3.** Trajectory characteristics (equation 38) for the SCZ and tachocline. The transition radius, shown as a dotted line, is 0.77 of the surface radius, and we have chosen  $kr_T = 3$ . The curves, which are here displayed well beyond their relevant physical domain, are everywhere regular and have continuous first derivatives at  $r = r_T$ .

Equations (38) and (42) for the characteristics and isorotation contours, respectively, comprise the interior tachocline solution for  $\Omega(r, \theta)$ .

Note that we have not made use of any inner boundary condition enforcing uniform rotation at a particular location marking the beginning of the radiative zone. In principle, this location is part of what determines the form of the  $T(r, \theta)$  stress. In practice, however, the simple model that we have adopted reproduces the helioseismology data so well that we may just stop the calculation at a value of  $r$  near 0.7. The isorotation contours at this point are very nearly spherical (cf. Fig. 4).

### 2.6.3 Modelling the Sun

At a transition radius of  $r_T = 0.77r_0$ , the helioseismology data show a modification of what we refer to in this paper as the ‘exterior’ solution. This translates to

$$\xi_1 = 1.75233, \quad \xi_2 = 0.26285, \quad \xi_3 = 1.28539, \quad \xi_4 = 0.060456. \quad (47)$$

The quantity  $(\Omega^2 - \Omega_1^2)/\Omega_2^2$  is simply  $\sin^2\theta_0$ , where  $\theta_0$  is the surface colatitude angle of the isorotation curve. Plots of the resulting characteristics and isorotation contours are shown in Figs 3 and 4 for the case  $kr_T = 3$ .

These figures are remarkable. The characteristics in Fig. 3 are everywhere smooth and regular. They are identical to isorotation contours for  $r > r_T$  and bear no resemblance to them for  $r < r_T$ . The corresponding isorotation contours (Fig. 4) are continuous, but have sharply discontinuous first derivatives at  $r = r_T$ . What is astonishing, however, is the extent to which they resemble the helioseismology GONG data (cf. Fig. 2). Recall that our model consists, in its entirety, of (i) the assumption of co-spatial surfaces of constant residual entropy and angular velocity in the TWE and (ii) local spatial forcing via an inhomogeneous term proportional to  $P_2(\cos\theta)$  that turns on at  $r = r_T$ . There is nothing else. Indeed, to keep the mathematics as simple as possible, we have not even used the best fit for the exterior solution shown in Fig. 2, but rather something much more basic. Still, the similarity of our closed-form solution to the GONG data is unmistakable.

Our results can be compactly summarized. The analysis shows that the SCZ is essentially in thermal wind balance from near the surface down to a transition radius of  $r_T = 0.77r_0$ , at which point distinctly quadrupolar tachocline meridional stresses bring the rotation profile to that of a solid body. For all of its detailed complexity, the role of turbulent angular momentum transport in the SCZ is strictly constrained, much as thermal transport has little choice but to establish a nearly adiabatic temperature profile.

## 3 CONCLUSION

The level of dynamical detail that can now be elucidated in numerical simulations of the SCZ is truly impressive (e.g. Miesch et al. 2008), but simulations incorporating the tachocline into global models of solar differential rotation are only just beginning to take form (Browning et al. 2006; Miesch et al. 2009). The solar tachocline remains a complex, poorly understood region of turbulent activity. While the details of the interaction between the tachocline and the large-scale differential rotation of the SCZ are not yet within reach, certain gross features of this interaction may in fact be tractable. In this paper, we have made an inroad by assuming that entropy is well mixed in surfaces of constant

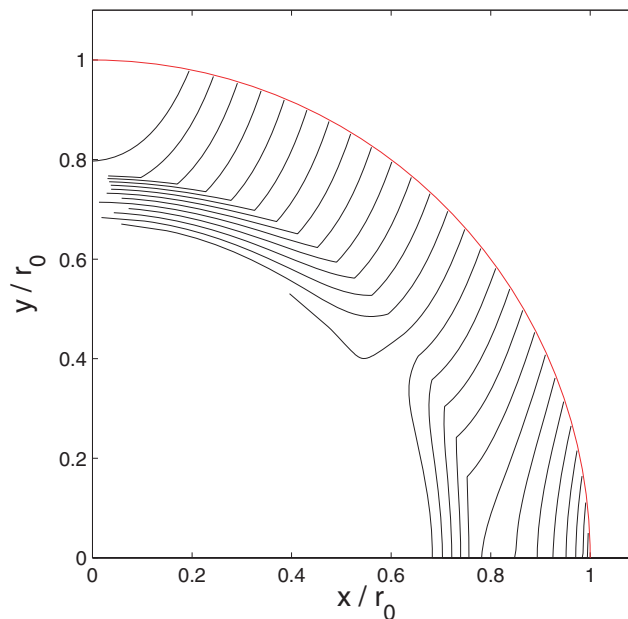


**Figure 4.** Isorotation contours (equation 42), with  $r_T = 0.77r_0$ ,  $kr_T = 3$ . The curves are continuous at  $r_T$  but have discontinuous first derivatives. The ensemble of isorotational contours bears a clear and striking resemblance to the helioseismology GONG data (cf. Fig. 2).

angular velocity within the convectively unstable portion of the tachocline, just as it appears to be within the SCZ. Since the convective Rossby number is likely to be even smaller here than in the SCZ, this would seem to be a reasonable approximation.

The explicit separation of the more general tachocline stresses from the mean inertial and baroclinic terms in the governing equation of vorticity conservation in its developed thermal wind form, and their reduction to a single formal inhomogeneous forcing term, has proven to be mathematically advantageous. The precise nature of this stress is, of course, of an unknown character. We would argue, however, that its consequences are not *unknowable*. The stress operates locally in radius and exhibits a definite quadrupolar angular structure: this is a very important point we wish to emphasize. It can be put to good use because the formalism of quasi-linear partial differential equations may be brought to bear on the problem. In particular, one may analyse the problem in terms of trajectory characteristics, whose form depends only implicitly on the tachocline stress terms, and solution characteristics, along which  $\Omega$  changes explicitly due to these same terms.

In BBLW theory, the solution characteristics convey constant  $\Omega$  along the trajectory characteristics. These characteristics are then identical to the isorotation contours. It is thus of considerable interest that in a simple and revealing class of solutions, the trajectory characteristics are mathematically identical to those of BBLW theory, even within the tachocline. The solution characteristics are certainly altered, however: they dictate that  $\Omega$  is initially constant along the trajectories, but then changes rapidly along these same curves as the tachocline is penetrated from above. The result is quasi-spherical isorotation contours inside of the tachocline, followed by a sharp upturn when the convection zone is reached from below. This behavior is also clearly seen in a more sophisticated, but still explicit, solution that is presented in this paper (cf. Fig. 4).

The radially local nature of the tachocline stresses is the crux of the problem, as it allows for mathematical modelling independent of the need of detailed knowledge of the spatial structure of the forcing. The simplest approach is to use Green's function techniques with forcing by a Dirac delta function at a transition radius  $r_T$ . The dominant  $P_2(\cos \theta)$  angular structure of the tachocline stresses becomes very apparent when the radial behavior is simplified in this way. Since the monopole response is evidently small, a reasonable surmise is that the turbulent stresses in the tachocline are driven by off-diagonal terms in a correlation tensor.

Angular momentum stresses within the SCZ create differential rotation, even if the initial condition is one of uniform rotation. Thus, in a causal sense, the tachocline likely owes its existence to the stresses of the convective zone, and not vice versa. In its current state of development, our calculation cannot directly address this causal link, but it does suggest how a dynamical couple arises between the surface spread in angular velocity and the tachocline angular velocity jump. This characteristic-based connection between the jump in the angular velocity at the tachocline and the spread of angular velocities at the solar surface is an important consequence of simple quadrupolar forcing.

Venturing even a little beyond a simple Green's function approach gives a much richer return. If one allows both an  $\Omega$  dependence in our  $f'$  function and a finite thickness for the transition region, the mathematical structure of the problem becomes more complicated: the solution and trajectory characteristics are now coupled. But it is still possible to obtain an explicit closed-form solution for the isorotation contours. This, the principal result of this paper, is shown in Fig. 4. The relatively simple solution so much resembles the GONG contours seen in Fig. 2; there can be little doubt that at the very least, the mathematical content of our approach is sound. Even if viewed at a purely phenomenological level, this is surely progress.

While our results provide a simple framework to aid in the elucidation of the global character of solar differential rotation, many questions remain unanswered. Quite apart from the grand challenge problem of tachocline structure and dynamics, it is legitimate to question

the work presented here on its own terms. How general and robust, for example, is the separation embodied in equation (5), or the critical assumption that a functional relation remains between residual entropy and angular momentum in the lower buoyancy tachocline? Why should such a simple approach work so well? There is also evidence that the tachocline thickness varies with  $\theta$  (Christensen-Dalsgaard & Thompson 2007), an effect completely neglected here. The relative simplicity of our arguments is somewhat deceptive because it masks the deeper conceptual problem of understanding precisely *how* the coupling between the tachocline and the convective zone rotation profile is established (see e.g. Rempel 2005; Gough 2010). These issues certainly have not been addressed in this paper; doing so without recourse to turbulence modelling will remain the province of numerical simulation for the foreseeable future.

But in this weakness also lies some power. We have noted earlier that the SCZ adiabatic temperature profile sheds little light on the dynamics of convective transport, though it is in an important sense completely beholden to it. This is not usually viewed as a shortcoming; rather it is a useful and powerful constraint. This is a point worth remembering: some aspects of the solar rotation problem are bound to be less mysterious than others. If thermal wind balance and the confluence of isorotation and constant residual entropy surfaces lead to important constraints for the Sun's rotation profile, the theorist's task will be greatly simplified – and understanding how the Sun rotates may prove to be a less daunting challenge than it might have first appeared.

## ACKNOWLEDGMENTS

This work benefited from an exceptionally thorough and constructive review by our referee Mark Miesch and we are most grateful to him for many valuable comments. We are likewise indebted to Nigel Weiss for important advice in the early stages of this work. Finally, we thank Rachel Howe for making reduced GONG data available to us in electronic form. This work has been supported by a grant from the Conseil Régional de l'Île de France.

## REFERENCES

- Balbus S. A., 2009, MNRAS, 395, 2056 (B09)  
 Balbus S. A., Weiss N. O., 2010, MNRAS, 404, 1263  
 Balbus S. A., Bonart J., Latter H., Weiss N. O., 2009, MNRAS, 400, 176 (BBLW)  
 Browning M. K., Miesch M. S., Brun A. S., Toomre J., 2006, ApJ, 648, L157  
 Christensen-Dalsgaard J., Thompson M. J., 2007, in Hughes D., Rosner R., Weiss R. N., eds, *The Solar Tachocline*. Cambridge Univ. Press, Cambridge, p. 53  
 Gough D. O., 2010, in Hasan S. S., Rutten R. J., eds, *Magnetic Coupling Between the Interior and the Atmosphere of the Sun*. Springer-Verlag, Berlin  
 Gough D. O., McIntyre M. E., 1998, Nat, 394, 755  
 Hughes D., Rosner R., Weiss R. N., eds, 2007, *The Solar Tachocline*. Cambridge Univ. Press, Cambridge  
 Miesch M., 2005, Living Rev. Sol. Phys., 2, 1 ([www.livingreviews.org/lrsp-2005-1](http://www.livingreviews.org/lrsp-2005-1))  
 Miesch M. S., Toomre J., 2009, Ann. Rev. Fluid Mech., 41, 317  
 Miesch M. S., Brun A. S., Toomre J., 2006, ApJ, 641, 618  
 Miesch M. S., Brun A. S., De Rosa M. L., Toomre J., 2008, ApJ, 673, 557  
 Miesch M. S., Browning M. K., Brun A. S., Toomre J., Brown B. P., 2009, in Dikpati M., Arentoft T., González Hernández I., Lindsey C., Hill F., eds, ASP Conf. Ser. Vol. 416, *Solar-Stellar Dynamos as Revealed by Helio- and Asteroseismology*. Astron. Soc. Pac., San Francisco, p. 443  
 Rempel M., 2005, ApJ, 622, 1320  
 Schwarzschild M., 1958, *Structure and Evolution of the Stars*. Dover Press, New York  
 Spiegel E. A., Zahn J.-P., 1992, A&A, 265, 106  
 Thompson M. J., Christensen-Dalsgaard J., Miesch M. S., Toomre J., 2003, ARA&A, 41, 599

This paper has been typeset from a  $\text{\TeX}/\text{\LaTeX}$  file prepared by the author.